Genome sequencing of 196 *Treponema pallidum* strains from six continents reveals additional variability in vaccine candidate genes and dominance of Nichols clade strains in Madagascar

Nicole A.P. Lieberman[1], Michelle J. Lin[1], Hong Xie[1], Lasata Shrestha[1], Tien Nguyen[1], Meei-Li Huang[1], Austin M. Haynes[2], Emily Romeis[2], Qian-Qiu Wang[3,4], Rui-Li Zhang[5], Cai-Xia Kou[3,4], Giulia Ciccarese[6], Ivano Dal Conte[7], Marco Cusini[8], Francesco Drago[6], Shu-ichi Nakayama[9], Kenichi Lee[9], Makoto Ohnishi[9], Kelika A. Konda[10,11], Silver K. Vargas[10], Maria Eguiluz[10], Carlos F. Caceres[10], Jeffrey D. Klausner[11], Oriol Mitjà[12,13], Anne Rompalo[14], Fiona Mulcahy[15], Edward W. Hook[16], Sheila A. Lukehart[2,17], Amanda M. Casto[2,18], Pavitra Roychoudhury[1,18], Frank DiMaio[19], Lorenzo Giacani[2,17], and Alexander L. Greninger[1,18*]

[1]Department of Laboratory Medicine and Pathology, University of Washington, Seattle, Washington, USA

[2]Department of Medicine, Division of Allergy and Infectious Diseases, University of Washington, Seattle, Washington, USA

[3]Institute of Dermatology, Chinese Academy of Medical Science & Peking Union Medical College, Beijing, China

[4]National Center for STD Control, China Centers for Disease Control and Prevention, Nanjing, China

[5]Department of Dermatology, The Second Affiliated Hospital of Nanjing Medical University, Nanjing, China

[6]Health Sciences Department, Section of Dermatology, San Martino University Hospital, Genoa, Italy

[7]STI Clinic, Infectious Diseases Unit, University of Turin, Turin, Italy

[8]Fondazione IRCCS Ca' Granda, Ospedale Maggiore Policlinico, Milan, Italy

[9]Department of Bacteriology I, National Institute of Infectious Diseases, Tokyo, Japan

[10]Unit of Health, Sexuality and Human Development and Laboratory of Sexual Health, Universidad Peruana Cayetano-Heredia, Lima, Peru

[11]Keck School of Medicine, University of Southern California, Los Angeles, California, USA

[12]Fight Aids and Infectious Diseases Foundation, Hospital Germans Trias i Pujol, Barcelona, Spain

[13]Lihir Medical Centre-International SOS, Lihir Island, Papua New Guinea

[14]Department of Infectious Diseases, Johns Hopkins Medical Institutions, Baltimore, Maryland, USA

[15]Department of Genito Urinary Medicine and Infectious Diseases, St James's Hospital, Dublin, Ireland

[16]Department of Medicine, University of Alabama, Birmingham, Birmingham, Alabama, USA

[17]Department of Global Health, University of Washington, Seattle, Washington, USA

[18]Vaccine and Infectious Disease Division, Fred Hutchinson Cancer Research Center, Seattle, Washington, USA

[19]Department of Biochemistry, University of Washington, Seattle, Washington, USA

*corresponding author

Email: agrening@uw.edu

Abstract

In spite of its immutable susceptibility to penicillin, *Treponema pallidum* (*T. pallidum*) subsp. *pallidum* continues to cause millions of cases of syphilis each year worldwide, resulting in significant morbidity and mortality and underscoring the urgency of developing an effective vaccine to curtail the spread of the infection. Several technical challenges, including absence of an *in vitro* culture system until very recently, have hampered efforts to catalog the diversity of strains collected worldwide. Here, we provide near-complete genomes from 196 *T. pallidum* strains – including 191 *T. pallidum* subsp. *pallidum* – sequenced directly from patient samples collected from 8 countries and 6 continents. Maximum likelihood phylogeny revealed that samples from most sites were predominantly SS14 clade. However, 99% (84/85) of the samples from Madagascar formed two of the five distinct Nichols subclades. Although recombination was uncommon in the evolution of modern circulating strains, we found multiple putative recombination events between *T. pallidum* subsp. *pallidum* and subsp. *endemicum*, shaping the genomes of several subclades. Temporal analysis dated the most recent common ancestor of Nichols and SS14 clades to 1717 (95% HPD: 1543-1869), in agreement with other recent studies. Rates of SNP accumulation varied significantly among subclades, particularly among different Nichols subclades, and was associated in the Nichols A subclade with a C394F substitution in TP0380, a ERCC3-like DNA repair helicase. Our data highlight the role played by variation in genes encoding putative surface-exposed outer membrane proteins in defining separate lineages, and provide a critical resource for the design of broadly protective syphilis vaccines targeting surface antigens.

Author Summary

Each year, millions of new cases of venereal and congenital syphilis, caused by the bacterium *Treponema pallidum* (*T. pallidum*) subsp. *pallidum,* are diagnosed worldwide, resulting in significant morbidity and mortality. Alongside endemic circulation of syphilis in low-income countries, disease resurgence in high-income nations has underscored the need for a vaccine. Due to prior technological limitations in culturing and sequencing the organism, the extent of the genetic diversity within modern strains of *T. pallidum* subsp. *pallidum* remains poorly understood, hampering development of a broadly protective vaccine. In this study, we obtained 196 near-complete *T. pallidum* genomes directly from clinical swabs from eight countries across six continents. Of these, 191 were identified as *T. pallidum* subsp. *pallidum*, including 90 Nichols clade genomes. Bayesian analysis revealed a high degree of variance in mutation rate among subclades. Interestingly, a Nichols subclade with a particularly high mutation rate harbors a non-synonymous mutation in a putative DNA repair helicase. Coupling sequencing data with protein structure prediction, we identified multiple novel amino acid variants in several proteins previously identified as potential vaccine candidates. Our data help inform current efforts to develop a broadly protective syphilis vaccine.

Introduction

Syphilis, caused by the spirochete bacterium *Treponema pallidum* subspecies *pallidum* (TPA) remains endemic in low-income countries, where the majority of cases of this infection occurs. A surge in syphilis incidence, however, has been recorded as well in mid- and high-income nations, primarily among men who have sex with men (MSM) and persons living with HIV (PLHIV). The United States saw a 6.5-fold increase in primary and secondary syphilis cases between 2000 and 2019 (1,2), driven in large part by cases among MSM, although cases among heterosexual individuals are now rising rapidly as well. Globally, there were approximately 6 million new cases per year among 15-49 year olds in 2016 (3). One million of these cases occur in pregnant women, of which 63% are in sub-Saharan Africa alone (4). Preventing cases among women of childbearing age is a critical worldwide public health initiative, as TPA can cross the placenta and cause spontaneous abortion and stillbirth. Maternal-fetal transmission of syphilis caused approximately 661,000 adverse birth outcomes globally in 2016 alone (5). In the United States, congenital syphilis is also rising, from 9.2 per 100,000 live births in 2013 to 48.5 per 100,000 live births in 2019, more than a five-fold increase (2).

Given rising infection rates, increasing difficulties in procuring benzathine penicillin G (BPG) for treatment (6), and widespread *T. pallidum* resistance to azithromycin (7–9) which is no longer a viable alternative to BPG, the development of a vaccine against syphilis has become a public health priority. To this end, the syphilis spirochete poses a particular challenge. In contrast to other gram-negative bacteria, TPA has a remarkably low surface density of integral outer membrane proteins (OMPs) (10,11) and uses phase variation (random ON-OFF switching of expression) to further vary its overall surface antigenic profile (12,13). In parallel, this pathogen has evolved a highly efficient gene conversion-based system able to generate millions

of variants of the putative surface-exposed loops of the TprK OMP, thus creating an ever-changing target for the host defenses, which fosters immune evasion, pathogen persistence, and re-infection (14–16). Furthermore, TPA cannot be cultured in axenic culture, instead requiring propagation in rabbit testes or, more recently, in co-culture with rabbit epithelial cells (17). This has further hampered efforts to sequence clinical specimens to catalog regions of conservation and diversity, particularly of the OMPs, which is critical for development of an effective vaccine. As of this writing, consensus sequences of only 67 TPA strains have been deposited in INSDC databases, and of these not more than 53 were recovered directly (or following low passage rabbit culture) from clinical specimens. Additional data exist within the Sequence Read Archive (SRA) for up to 600-800 samples annotated as TPA but, without extensive manual curation and reliable assembly pipelines, high-quality data contained within the SRA remain inaccessible to most users. To inform vaccine development efforts, we generated high quality (<1% ambiguous or missing data) near-complete genomes from 196 *T. pallidum* genomes using hybrid capture, enabling direct determination of sequences from clinical specimens without the need for enrichment by culture in rabbits or *in vitro*. These newly available genomes were analyzed to unveil diversity in potential TPA vaccine targets in combination with *in silico* protein folding technology. Our work broadens our understanding of the molecular underpinnings of TPA, and serve as a resource for developing a broadly protective vaccine effective against syphilis.

Results

Nichols clade strains are predominant in Madagascar

As part of ongoing efforts to catalog global *T. pallidum* genomic diversity, we received samples containing *T. pallidum* genomic DNA recovered from primary or secondary lesions. We

attempted whole genome sequencing on those with > 100 copies of *tp0574* per 17.5 µL genomic DNA and obtained 196 high quality genomes consisting of <1% ambiguities using a custom hybridization capture panel to enrich for *T. pallidum* DNA followed by processing through a custom bioinformatic pipeline for consensus genome calling involving both de novo assembly and reference mapping to the SS14 reference genome (NC_021508.1). Summary demographic characteristics for all samples, including 191 TPA, four *T. pallidum* subsp. *endemicum* (TEN), and one *T. pallidum* subsp. *pertenue* (TPE) used in this study are presented in Table 1. Samples were collected between 1998 and 2020 from 8 countries (Peru, Ireland, USA, Papua New Guinea, Madagascar, Italy, Japan, and China) across 6 continents. Median coverage of the reference genome by trimmed, deduplicated reads was 76.8x (range 16.5 - 1293.4), with a minimum of 6 reads required to unambiguously call a base. Median input genomes, as determined by *tp0574* qRT-PCR, for successful genome recovery was 4,319 copies (range 101 – 304,484) (Supporting Information 1 – Sample Statistics). The median number of ambiguities in the finished genomes prior to masking was 49 (range 0-10,753).

Table 1: Demographic information of samples sequenced in this study

Country	Year(s) of Collection	Number of Samples	Sex (n)			Stage (n)			Previous Study
			Male	Female	Unknown	Primary	Secondary	Unknown	
Peru	2019	9	5	0	4	5	0	4	n/a
Ireland	2002	11	0	0	11	0	0	11	(18–20)
USA	1998-2002	15	11	3	1	14	1	0	(19,20)
Papua New Guinea	2019	1	0	0	1	0	0	1	n/a
Madagascar	2000-2007	85	0	0	85	10	16	59	(20–22)
Italy	2017	10	10	0	0	10	0	0	n/a
Japan	2019-2020	57	34	22	1	0	0	57	n/a
China	2018	8	0	0	8	0	0	8	n/a
TOTAL	***1998-2020***	***196***	***60***	***25***	***111***	***39***	***17***	***140***	

Following the assembly of the 196 genomes, we combined our strains with an additional 55 publicly available consensus genomes, including five TPE, two TEN, 11 TPA laboratory isolates highly passaged in rabbit, and 37 direct clinical specimens/low passage rabbit TPA strains. Due to differences in library preparation expected to affect performance of our assembly pipeline, we chose not to reassemble genomes that did not have an available consensus sequence. All genomes were masked at the intra-rRNA tRNA-Ala and tRNA-Ile and highly repetitive *arp* and *tp0470* genes for which short read Illumina sequencing could not resolve position or relative length. Genomes were further masked at all paralogous *tpr* genes prior to recombination masking by Gubbins (23).

The maximum-likelihood phylogenetic tree shown in Figure 1 (and in tabular format in Supporting Information 1 – Sample Metadata) is defined by approximately 130-150 non-recombining SNPs separating any two Nichols and SS14 tips and approximately 1,200-1,450 SNPs separating any two TPA and TPE or TEN tips. It recapitulates several features seen in previous phylogenies of *T. pallidum*. Notably, it includes a SS14 Omega node that contains nearly all SS14 clade samples, as well as tight geographic clustering of samples predominantly collected in China and Japan (24) and characterized by uniform azithromycin resistance caused by the A2058G mutation in the 23S rRNA allele (Figure 1A-C; SS14 Omega – East Asia node). None of these samples was resistant via the A2059G allele. We also observed genotypic azithromycin resistance in geographically diverse samples in both the SS14 and Nichols clades, further supporting the hypothesis that this mutation arises spontaneously (24).

The most striking feature of our *T. pallidum* phylogeny is the extensive circulation of strains belonging to the Nichols clade in Madagascar. All but one of the 85 Madagascar strains belonged to one of two Nichols subclades, A and B. The former consists of only Madagascar

171 strains except for a single strain from Cuba, and the latter containing only Madagascar samples.
172 Except for an A2059G 23S rRNA mutation (25) observed in one sample, all Madagascar Nichols
173 strains were azithromycin sensitive.

174 In addition to Nichols subclades A and B primarily from Madagascar, three additional
175 distinct subclades were observed, containing samples collected throughout the world. The
176 Nichols C subclade shares a common ancestor with the Nichols B subclade and is uniformly
177 azithromycin resistant, in contrast to most other Nichols clade samples. Both Nichols D (which
178 contains all laboratory strains) and Nichols E subclades are more distantly related to the
179 Madagascar samples in Nichols A and B. The Nichols E subclade includes two previously
180 reported samples from France as well as two newly sequenced samples from Japan and Italy.
181 Interestingly, both the Japanese and Italian patients whose samples are included in this subclade
182 report their sexual orientation as MSM; one French sample, CW59, was collected from an anal
183 smear. Although this is hardly conclusive, the appearance of distinct TPA clades circulating
184 among MSM individuals has recently been documented in Japan (26), suggesting that this
185 phenomenon may be occurring worldwide.

186 In addition to the unexpected number of Nichols clade samples, we were also surprised to
187 observe two samples from Maryland that clustered with the very distant SS14 clade genome,
188 MexicoA, originally collected in 1953 from a male living in Mexico. These strains, MD06 and
189 MD18B, diverge from the MexicoA strain by 33 and 24 non-recombining SNPs, respectively;
190 from SS14 Omega strains by about 45 SNPs; and Nichols clade strains by about 150 SNPs. The
191 MexicoA strain is unique in that it shares signatures of both syphilis and yaws organisms in
192 several virulence factors (27,28). To our knowledge, clinical specimens clustering with the
193 MexicoA strain have not previously been reported. Although the MD18B and MD06 samples

194 were collected in 1998 and 2002, respectively, and little demographic information for the
195 samples exists, this is further evidence that our definitions of subspecies of *T. pallidum* may need
196 periodic revisiting.

197 We also found that four Japanese samples that were clinically diagnosed as syphilis but,
198 based on our whole genome analysis, appear to be part of the TEN subspecies, sharing an
199 ancestor with the canonical TEN genomes IraqB and BosniaA. The observation of TEN samples
200 following a syphilis diagnosis has been previously reported in Japan (29), Cuba (30), and France
201 (presumed to have been contracted in Pakistan) (31). While both the previously discovered and
202 new Japanese TEN samples are resistant to azithromycin via the canonical mutation in the 23S
203 rRNA alleles, neither the Cuban nor French samples are resistant. Furthermore, three of the four
204 samples reported herein were collected from individuals with diverse travel histories (China,
205 Japan, and the Philippines), suggesting that a sexually transmitted TEN outbreak may be even
206 more widespread than previously suspected.

207 As a mechanism to begin cataloging diversity of several genes known to be polyallelic,
208 we also examined the multi-locus sequence type (MLST) types (32) of all TPA samples using
209 whole genome sequence as well as the combined MLST. Figure 1D highlights the six most
210 common MLST at each locus for TPA samples and whether the overall subtype had been
211 previously reported. Complete MLST data can be found in Supporting Information 1. Across all
212 238 TPA samples, we found a total of 15 unique complete *tp0136* sequences, including six not
213 previously reported in the MLST database, which contains 26 alleles. Seventeen unique *tp0548*
214 sequences were found, including seven novel sequences, relative to 58 known alleles. All five
215 observed *tp0705* alleles had been previously reported. In total, excluding the 13 samples that
216 were indeterminate at any of the three loci, we found a total of 40 unique haplotypes, including

22 not previously reported in the MLST database. Overall, 88 of 225 *T. pallidum* subsp. *pallidum* samples had a novel overall haplotype, including at least one sample from each country from which samples were obtained, and all 76 (100%) from Madagascar, underscoring the importance of wide geographic sampling to catalog the diversity of TPA strains.

Putative recombination shapes modern *T. pallidum* subsp. *pallidum* genomes but remains a rare event

Although *T. pallidum* does not have any known plasmids or infecting phages, recombination has nonetheless been shown to be an important mechanism by which genetic diversity may be generated in this pathogen (27,33,34). In particular, the *tpr* family of paralogs is thought to have arisen through gene duplication (28,35); for this reason, all *tpr* genes have been masked for all analyses in this study. Figure 2A shows the comparison of ML tree topology between genomes that have been recombination masked (left) or unmasked (right) (with tip order included in Supporting Information 2). Although no samples were classified to different subclades when recombinant loci were not masked, the overall tree topology was altered. Notably, the SS14 Omega node had more distinct subclades in the absence of recombination masking, suggesting that much of the diversity within SS14 Omega is due to recombination rather than mutation. Furthermore, the Nichols B subclade of Madagascar samples becomes the outgroup within the Nichols clade in the absence of recombination masking.

The method of recombination detection we employed relies on identification of an increased density of SNPs per sliding window throughout the clonal frame rather than identification of a discrete donor for each putative recombination event. Although previous analyses have found more recombination in the Nichols clade than SS14 (33), our use of more

than 90 clinical specimens belonging to multiple Nichols subclades, albeit with a geographic bias, likely provides a more complete picture of the evolutionary processes that shaped the Nichols clade. In spite of the number of samples examined, recombination remained a rare event in Tpr-masked genomes. Of the 474 nodes on the ML tree, including 238 tips and 236 internal nodes, only 27 branches with recombination were detected. Sixteen of these were on internal nodes and 11 on extant. Of the extant recombination events, four were detected in the 101 Nichols clade samples, and seven of 137 in the SS14 clade samples, suggesting no clade-specific differences in recombination (p=0.7633, Fisher's Exact test).

Figure 2B highlights the positions of identified recombinant regions in the aligned genomes, with grey blocks corresponding to recombination that occurred during the separation of SS14 and Nichols clades, and colored blocks corresponding to recombination events that occurred during the evolution of individual subclades. The grey and red striped block represents a second recombination event in the SS14 Mexico clade that occurred in the same region as the ancestral recombination. As has been previously reported (33,36), many of the identified recombinant regions correspond to the most diverse genes in *T. pallidum*, such as *tp0136*, *tp0326 (BamA)*, and *tp0515 (LptD)* (Supporting Information 2). Notably, many of the ORFs identified as recombinant encode proteins that are predicted to be at least partially surface exposed, and therefore the increased SNP density may represent either bona fide recombination or selective pressure of the host immune system on non-recombinant genes.

Recombination events specific to each subclade shown in Figure 2B were examined, with representative data in Figure 2C-F for SS14 Mexico, Nichols A, Nichols B, and Nichols E subclades, respectively. Windows of approximately 60 bases of the alignments of putative recombinant regions are shown, and include additional *T. pallidum* species members TPE, TEN,

and the *T. pallidum* Fribourg-Blanc treponeme, recently proposed to be reclassified as a TPE strain, due to its genetic similarity to other yaws strains (37), with non-identical nucleotides highlighted. Interestingly, several of the identified recombinant loci, including Block G in SS14 Mexico, Block F in Nichols A, and Blocks E and L in Nichols E, have sequences identical to those found in all 6 TEN genomes included in Figure 1. TEN or TPE sequences have been found previously in several Nichols clade samples, suggesting prior recombination (33,36). However, our markedly extended phylogeny of the Nichols clade suggests that recombination between TPA and TEN has independently occurred on multiple occasions. This demonstrates that inter-subspecies recombination continues to play an important role in the diversification of *T. pallidum* subspecies.

T. pallidum subsp. _pallidum_ subclades have different rates of SNP accumulation

The evolutionary history of TPA has been a point of considerable debate in recent years, particularly in light of new evidence that could not exclude the presence of TPA in Northern Europe in the late 15th century, casting doubt on the popular theory that venereal syphilis was introduced to Europe by the returning Columbian expeditions (36). In order to determine the date of the most recent common ancestor (MRCA) of the samples included in our study, we first analyzed the temporal signal present among TPA strains by regressing the root-to-tip distances in the SNP-only maximum-likelihood tree (Figure 3A). The left panel shows this calculation performed on a tree that included 11 highly passaged laboratory strains (eight in Nichols clade and three in SS14 clade), identified by open circles, while the right panel is based on a tree that excluded laboratory strains. Notably, the negative slope seen for the Nichols clade appears to be due to the presence of laboratory strains. This is consistent with accelerated accumulation of

SNPs during routine passage of the laboratory strains for decades between collection and sequencing. Therefore, laboratory strains were excluded from further dating analysis.

We were curious as to why the Pearson correlation coefficients of the SS14 and Nichols clades (0.200 and 0.023, respectively) were so poor even in the absence of laboratory strains, and hypothesized that this may be due to differences inherent to the polyphyletic structure of both clades. We tested this by plotting the residuals of the regression by subclade and found significant differences between groups (Figure 3B, $p < 2e^{-16}$, ANOVA), suggesting that rates of SNP accumulation may differ across the TPA phylogeny.

Therefore, we proceeded to Bayesian ancestral reconstruction and dating of clinical specimens by BEAST 2 (38), using an uncorrelated relaxed clock with a starting rate of $3.6x10^{-4}$ (24,39) as a prior model to account for differences in rates of mutation in different branches of the tree. Figure 3C shows the dated Bayesian phylogeny, with branches colored to reflect the rate of SNP accumulation. Black nodes have a posterior probability of >95%. Consistent with previous studies (24,36,39), we dated the MRCA of TPA to 1717 (95% HPD 1543-1869), the Nichols clade to 1893 (1839-1940), and the SS14 clade to 1921 (1868-1964), and found that the rates of SNP accumulation on branches with >95% posterior probability ranged between 0.2 and 0.73 fixed SNPs/year. The inset figure shows the mean rates of diversification on branches with >95% posterior support for each tip, supporting our hypothesis that different subclades have different rates of mutation ($p < 2e^{-16}$, ANOVA).

Host immune pressure drives mutation in the same putative antigens in SS14 and Nichols clades

Observed differences in accumulation of SNPs among subclades may represent the effects of sampling bias or bottlenecks or may reflect differences in the underlying biology. To examine the functional differences that define each subclade (including loci identified as recombinant (Figure 2), we used augur (40) to reconstruct the ancestral nodes identified in the recombination-masked ML phylogeny, transferred ORF annotations from the TPA reference genome NC_021508.1, and translated each ORF to detect coding changes. Figure 4A shows all nodes used for these analyses, with subclade tips collapsed for simplicity. All coding changes detected in Node 101 (SS14 clade ancestral) relative to Node 001 (Nichols clade ancestral, considered equivalent to the TPA root node for these calculations) are shown; data for all additional parent-child node pairs are included in Supporting Information 3. Forty-nine of 1002 putative ORFs were altered between SS14 and Nichols ancestral nodes, with a total of 134 non-synonymous mutation events. We defined a mutation event as a single amino acid change, insertion/deletion, or frameshift. We did not separately include the effects of putative recombination events because we did not attempt to formally characterize recombination donors, and therefore could not disentangle the effects of recombination from selective pressure driving increased mutation.

We next attempted to define functional changes between the SS14 and Nichols clades by examining overrepresentation of altered loci in categories annotated by structural similarity (41). We used the annotation of the Protein Data Bank (PDB) structure of the highest scoring model, with a confidence cutoff of 75%, allowing 798 coding sequences (CDSs) to be assigned to a total of 62 unique PDB categories. We then performed Fisher's exact tests to test for overrepresentation of altered proteins in each category. For SS14 vs Nichols ancestral nodes (101 vs 001, Supplementary Figure 1), we only found significant overrepresentation in a single

category, “Signaling Protein”, with 3 (*tp0073*, *tp0640*, and *tp0995*) loci out of the 16 in the category altered. However, because these annotations are by structural similarity rather than known function, it is likely that testing for overrepresentation of structural annotations does not fully capture the functional differences between any two clades.

Because functional annotation of *T. pallidum* proteins is still hampered by the absence of a reverse genetics system, we chose next to focus on alteration of proteins known or suspected to interact with the host immune system. We included proteins that reacted with pooled sera from individuals with known syphilis infection (42,43) or otherwise known to be surface-exposed (Supporting Information 3 - Antigens) and again performed overrepresentation tests (Figure 4B). Along branches with more than 10 altered proteins, only two nodes (N015, Nichols C, and N005, Nichols D Lab Strains) did not have significant p values ($p<0.05$) relative to their parent. When examining individual mutation events in nodes with more than four altered proteins, mutation in antigenic proteins represents more than 30% of the amino acid variability in more than half of nodes, and at least 10% in all nodes (Figure 4C). Antigenic proteins are enriched among proteins that become mutated relative to their parent node in multiple subclades, representing separate events (Figure 4D). Furthermore, among antigens that were mutated relative to the parent node in more than one subclade, none was exclusive to either the SS14 or Nichols clade. These data suggest that interaction with the host immune system drives a large proportion of the evolution of both major clades of this pathogen, either via individual SNPs or horizontal gene transfer.

However, although antigens are enriched for non-synonymous mutations relative to the rest of the proteome, mutation of non-antigenic proteins may make considerable contributions to *T. pallidum* pathogenicity and immune interaction. When examining proteins whose mutation was unique to a single clade (Figure 4D), we found a C394F mutation in the ERCC3-like DNA

repair helicase TP0380 (44) only in the Nichols A subclade, which had a much higher median rate of SNP accumulation than any other subclade (Figure 3C). It is plausible that mutation of this helicase compromises DNA repair and contributes to a more rapid rate of evolution within this clade.

Predicted structural changes of putative surface proteins not limited to polymorphic residues

For any protein, multiple independent mutation events along several branches of the TPA phylogeny strongly suggest the protein is under selective pressure. Of the six proteins that undergo mutation along four or more of the 14 branches in the phylogeny (Figure 4D and Supporting Information 3 – Heatmap), five (TP0136, TP0326, TP0548, TP0966, and TP0967) are known to be antigenic. TP0326, TP0548, TP0966, and TP0967 are likely outer membrane proteins based on their homology to *N. gonorrhoeae* BamA (TP0326) and *E. coli* FadL (TP0548) and TolC (TP0966, TP0967) (45) and reviewed in (46). TP0136 is a lipoprotein that appears to be localized to the outer membrane, where it functions as a fibronectin- and laminin-binding adhesin (47–49). To date, recombinant TP0136 and TP0326 have been tested as potential vaccine candidates in rabbits, with TP0136 delaying ulceration but not providing full protection upon challenge (47), and TP0326 providing partial protection in some studies (50,51), while not protective in others (52). Although antigens harboring polymorphisms would not traditionally be considered viable vaccine candidates, the paucity of outer membrane proteins in *T. pallidum* (46) demands evaluation of imperfect candidates.

Accordingly, for the five most frequently mutated putative outer membrane antigens, we developed models that highlight the positions predicted to undergo the most structural change

upon mutation, including those at orthogonal sites. We first performed global alignments of sequence variants for each of the five proteins using hhpred (53–55) (Supplementary Figures 2-6, panel A, and Supporting Information 4). We then generated composite homology models of the SS14 variant using RosettaCM (56) guided by hhpred sequence alignment. Ribbon structures and surface contours with highlighted polymorphic residues of the SS14 variant are shown in Supplementary Figures 2-6, panels B and C, respectively. Then, the SS14 model was used as a template for predicting the structure of variants of other strains. We performed a global superposition of variant structures and computed an average per-atom displacement relative to the reference model (taking sequence changes into account, see Methods). The resulting per-atom deviations were then mapped onto the model of the SS14 variant, with blue representing regions of the lowest displacement from the SS14 model and red the highest (Supplementary Figures 2-6, panel D). This approach allowed detection of structural changes not simply at the site of the polymorphism, but also orthogonal changes due to disruption of hydrogen and other bonds. Furthermore, it allows "tuning" of the structural effect of a mutation on each atom, with the mutation of similar residues (such as leucine to isoleucine) resulting in less displacement of each atom than substitution of dissimilar residues (such as arginine to histidine). N terminal residues comprising predicted secretion sequences are not shown for TP0136 (48) or TP0326 (57). Best estimates for Gram negative signal peptides were predicted by SignalP 5.0 (58) for TP0548, TP0966, and TP0967 SS14 variants and excluded from display.

In spite of slightly different approaches employed in their generation and our use of the SS14 variant rather than Nichols, our structural models for TP0326, TP0548, TP0966, and TP0967 generally agree with the models recently proposed by Hawley *et al.* (45). TP0326 is a large multidomain component of the β-barrel Assembly Complex (BAM) and includes a C-

terminal β-barrel. Consistent with previous studies (34,45,57,59), we found that extracellular loop (ECL)-4 and the serine-rich tract of ECL-7 contribute to much of the between-strain structural diversity (arrows and single arrowheads, respectively, Supplementary Figure 2B-D). We also found that the large ECL-3 (double arrowheads, Supplementary Figure 2B-D) had nine polymorphic residues, rendering the entire exposed surface of the protein variable due to strain-to-strain variation in ECLs, particularly 3, 4, and 7 (Supplementary Figure 2C-D).

In contrast to TP0326, the structure and function of which has been studied extensively, less is known about TP0548, a predicted homolog of the *E. coli* fatty acid transporter FadL. We predict the structure to be a 14-stranded β-barrel, with periplasmic C-terminal α-helices, consistent with previous studies (45). Prediction of linear B cell epitopes (BCEs) using BepiPred 2.0 (60) revealed that, depending on the as-yet unknown position of the cleavage of the N terminal signal sequence, up to four linear BCEs eight residues or longer are predicted to occur in invariant, extended host-facing loops at the N-terminus and ECL-2 (Supplementary Figure 3A, arrows in Supplementary Figure 3B show the relevant loops), rendering them potentially of use in a vaccine cocktail. Notably, the displacement seen in ECL-2, containing BCEs 3 and 4, (Supplementary Figure 3D, arrow) is most likely due to stochastic differences in predicting the conformation of the flexible loop rather than true structural variation.

Both TP0966 and TP0967 are predicted to be orthologs of the *E. coli* efflux pump TolC (45), and are predicted to have a tri-partite structure, with each monomer contributing four β-strands to β-barrel that spans the outer membrane with BCEs predicted within the ECLs (45). Supplementary Figures 4B and 5B highlight a single monomer for TP0966 and TP0967, respectively; both ECLs of TP0966, and ECL1 of TP0967, contain polymorphic residues that disrupt predicted linear B cell epitopes (Supplementary Figures 4A and 5A, Supplementary

Figures 4C and 5C, arrows). For both TP0966 and TP0967, the residues with the most displacement that disrupt the extracellular surface are not the polymorphic positions (Supplementary Figures 4D and 5D, arrows). Rather, in TP0966, the polymorphic charged residues in and adjacent to the ECLs may cause changes to electrostatic interactions that influence loop position. In TP0967, the length of the poly-glycine tract alters the position of ECL1. The likely result is disruption of the conformational epitopes formed by the surface loops in TP0966 and TP0967.

Finally, we generated a structural model of TP0136, and found it to adopt a 7-bladed beta-propeller fold in its N-terminal domain, followed by a relatively unstructured C-terminal domain (Supplementary Figure 6B). The beta-propeller structure is noteworthy as it is homologous to structures found in several eukaryotic integrins that mediate binding to the extracellular matrix (61), as well as to bacterial lectins (62). Several tracts of serine and lysine repeats are a unique structural feature of TP0136; the beta-propeller fold of TP0136 allows these intrinsically disordered regions to form unstructured loops between beta strands. Unsurprisingly, the surfaces that comprise the β-strands have some polymorphisms (Supplementary Figure 6B and C, boxed region) but they are not predicted to cause extensive structural displacement and disruption of the fold, as shown by primarily blue coloring in the boxed region of Supplementary Figure 6D.

Interestingly, the deletion in TP0136 that appears in 4 sequence variants (2, 5, 22, 23, and 24, Supplementary Figure 6A, alignment position 161-192) and entirely removes the large flexible loop annotated by an arrow in Supplementary Figure 6B-D is not found in any ancestral node sequences (Figure 4), but arises independently in strains from multiple geographic locations, including Nichols clade strains from Madagascar and the United States (subclades A,

B, and D), and SS14 clade strains from Japan, Peru, and Ireland (subclades Omega – East Asia and SS14 Omega`), consistent with this genomic region being a hotspot for recombination (Figure 2).

Discussion

In recent years, *T. pallidum* genomics has been significantly advanced by projects aimed at studying the origin and spread of strains responsible for the modern syphilis pandemic (24,26,36,39,63), as well as the emergence of azithromycin resistance (24,26,63). Increasingly the challenge in *T. pallidum* genomics will be attaining complete genomic sequences from undersampled regions, associating genomic sequencing with spirochete biochemical functions, and gaining actionable insights into *T. pallidum* evolution that inform vaccine design.

With these goals, we generated 196 near-complete *T. pallidum* genomes from diverse locations, including three countries – Peru, Italy, and Madagascar – with no previous complete genomes publicly available. Peruvian samples (n=9) belonged exclusively to the SS14 Omega` subclade, which contains samples collected worldwide and corresponds to the largest SS14 sub-lineage in a recent analysis of SNPs in TPA strains (63). Eight of the ten Italian strains also belonged to the Omega` subclade.

The remaining two Italian strains, collected in Turin and Bologna, were of two distinct Nichols subclades, one of which clustered with three Japanese syphilis strains in Nichols subclade C, and the other clustered with samples of Japanese and French origin, forming the distantly related Nichols subclade E. Notably, none of the Japanese or Italian samples clustered with the Malagasy Nichols samples, which, but for a single Cuban strain in Nichols subclade A, formed two private subclades. Because the samples from Madagascar were collected between

2000-2007, it is unknown whether there has been introduction of additional lineages of TPA in the intervening years, or whether the two nearly private subclades are reflective of the currently circulating strains.

Sample collection date is also an important consideration to the interpretation of azithromycin resistance data. None of the strains collected in the USA between 1998 and 2002 were resistant to azithromycin. However, this was prior to the detection of widespread azithromycin resistance in the United States (8); therefore, the lack of resistance detected in the strains sequenced for the present study should not be considered representative of the current status. Only one of the strains collected from Madagascar between 2000 and 2007 was resistant to azithromycin; no subsequent sampling has been performed, thus, no conclusions about azithromycin resistance in strains currently circulating in Madagascar can be drawn.

In our study, as in other recent global *T. pallidum subsp. pallidum* genomics initiatives (24,63), samples were collected and sequenced based on availability rather than representing an even distribution based on global burden of disease. The result of this is that, although we gained a broader picture of worldwide diversity, some regions (North America, western Europe, eastern Asia) continue to be overrepresented, while other regions (Africa – particularly Sub-Saharan Africa, which bears the largest share of cases worldwide – and South Asia and South America) are still vastly under-sampled. However, an important takeaway from our study as well as the recent paper from Beale *et al.* (63) is that the general understanding that SS14 represents the vast majority of circulating strains may require revisiting. Although the island nation of Madagascar is unlikely truly representative of the diversity of strains currently circulating in Sub-Saharan Africa, particularly because the samples are 15-20 years old, our finding that 99% of Malagasy strains belong to the Nichols clade, coupled with Beale *et al.*'s discovery of Nichols strains

492 circulating in Zimbabwe and South Africa (63) strongly suggests widespread circulation of
493 Nichols clade TPA in Africa. Clearly, increased sampling must be a priority to enable
494 understanding of syphilis epidemiology in Africa, and to ensure a vaccine covers strains
495 circulating in the regions most hard hit by the modern pandemic.

496 Our temporal analysis generally agreed with previous estimates of mutation rate (39,63)
497 in spite of the fact that we used a relaxed, rather than fixed, clock model to determine whether
498 there were differences in the rate of mutation along different branches of the *T. pallidum* subsp.
499 *pallidum* phylogeny, which could indicate either different selection pressures or underlying
500 biological differences contributing to the phenotype. Indeed, we found significant differences in
501 the rates of mutation among the subclades (Figure 3C). The Nichols A subclade was particularly
502 interesting to us, given its high median rate of mutation along branches within the subclade with
503 high posterior support. Notably, when we examined the non-synonymous mutations that defined
504 the Nichols A subclade relative to its ancestral node, shared by Nichols subclades A, B, and C
505 (Figure 4A/D), we found that one of the non-synonymous mutations found only within the
506 Nichols A subclade was in TP0380, a putative ERCC3-like DNA repair helicase that interacts
507 with DNA replication machinery by yeast two-hybrid analysis (41,44,64). Although the
508 functional significance of the C394F mutation (C1181A in *tp0380*) is unknown, it is tempting to
509 speculate that it may directly affect DNA repair. This hypothesis of a potential mutator
510 phenotype in *T. pallidum* can now be examined *in vitro*, given the recent description of the first
511 genetic transformation in *T. pallidum* (65). If TP0380 mutation is indeed responsible for the
512 elevated rate of mutation seen within the Nichols A subclade, the implications for vaccine design
513 may be significant.

514 By definition, an effective syphilis vaccine needs to protect against most strains
515 circulating where the vaccine is administered. Our work further supports that the majority of
516 non-synonymous mutations that define *T. pallidum* subsp. *pallidum* subclades are in proteins
517 putatively located in the outer membrane, or known to react with serum from syphilis patients
518 (Figure 4) (42,43). These data, along with recent structural modeling of *T. pallidum* outer
519 membrane proteins showing that putative B cell epitopes are primarily found on the protein
520 surface predicted to face the host (45), strongly suggest that immune pressure is the most
521 important driver of mutation in *T. pallidum* subsp. *pallidum*. Indeed, our own structural
522 modeling, which highlights regions with the highest structural displacement due to sequence
523 variability, confirms that the regions with the highest displacement are frequently polyallelic
524 (Supplementary Figures 2-6). Given the paucity of *T. pallidum* outer membrane proteins, and the
525 extensive mutation of predicted epitopes, a multivalent vaccination strategy may engender a
526 polyclonal humoral response capable of neutralizing a wider array of strains, a strategy currently
527 being adopted in our laboratory.
528 Finally, an important caveat to these data is that, due to their extensive recombination and
529 duplication, we excluded arguably the most important *T. pallidum* proteins that interact with the
530 host immune system, the Tpr family (14,28). Although this approach has been used before to
531 ensure an accurate phylogeny free from the confounding effects of recombination (24,63), as
532 well as to prevent mistakes due to improper resolution of their repetitive elements during de
533 novo assembly (39), an understanding of how the *tpr* genes evolve and influence host immunity
534 is critical to developing an efficacious vaccine to *T. pallidum*. Accordingly, we are currently
535 undertaking additional analyses of the Tpr family in these strains, including the hypervariable
536 regions of TprK.

The data presented in this study represent a step forward toward developing a successful vaccine against syphilis. Alongside increased sequencing of strains from regions without extensive sampling, particularly Africa and South America, improved biophysical and computational methods are necessary to unequivocally determine which proteins are expressed on the surface of the bacterium during human infection. The new system to genetically engineer *T. pallidum* (65) will undoubtedly aid these studies, as well as allow the development of strains to test vaccine candidates in animal experiments. Finally, a successful vaccine must not only be efficacious against all circulating strains, but must also be sufficiently low cost and robust to ambient temperatures to allow distribution in the developing world, which is currently bearing the burden of the modern pandemic.

Methods

Ethics Statement: All human samples were collected and deidentified following protocols established at each institution. Samples from Ireland, Madagascar, and USA have been previously published (18–22). IRB protocol numbers for collection of the remaining samples are as follows: China: Nanjing Medical University, 2016□050; Italy: Universities of Turin and Genoa, PR033REG2016, University of Bologna, 2103/2016; Japan: National Institute of Infectious Diseases, 508 and 705; Peru: University of Southern California, HS-21-00353; Papua New Guinea, Lihir Medical Center, Medical Research Advisory Committee of the PNG NDOH No: 17.19. Sequencing of deidentified strains was covered by the University of Washington Institutional Review Board (IRB) protocol number STUDY00000885.

Library Preparation: Samples were collected and DNA extracted using standard protocols (66). Treponemal burden was assessed by quantitative PCR (qPCR) for *TP47* multiplexed with human

β-globin, using primer sequences *TP47*-F: 5'-CAAGTACGAGGGGAACATCGAT, *TP47*-R: 5': TGATCGCTGACAAGCTTAGG, *TP47*-probe: 5'-6FAM-CGGAGACTCTGATGGATGCTGCAGTT-NFQMGB. Pre-capture libraries were prepared from up to 100 ng input genomic DNA using the Kapa Hyperplus kit (Roche), using a fragmentation time of 8 minutes and standard-chemistry end repair/A-tailing, then ligated to TruSeq adapters (Illumina). Adapter-ligated samples were cleaned with 0.8x Ampure beads (Beckman Coulter) and amplified with barcoded primers for 14-16 cycles, followed by another 0.8x Ampure purification.

***T. pallidum* capture**: Capture of *T. pallidum* genomes was performed according to Integrated DNA Technology's (IDT's) xGen Hybridization Capture protocol. Briefly, pools of 3-4 libraries were created by grouping samples with similar treponemal load for a total of 500 ng DNA, and Human Cot 1 DNA and TruSeq blocking oligos (IDT) added prior to vacuum drying. The hybridization master mix, containing biotinylated probes from a custom IDT oPool tiling across the NC_010741.1 reference genome, was then added overnight (>16 hr) at 65C. The following day, streptavidin beads were added to the capture reaction, followed by extensive washing, 14-16 cycles of post-capture amplification, and purification with 0.8x Ampure beads. Pool concentration was determined by Qubit assay (Thermo Fisher) and size verified by Tapestation (Agilent). Libraries were sequenced on a 2x150 paired end run on a HiseqX.

Fastq processing: Fastqs were processed and genomes assembled using our custom pipeline, available at https://github.com/greninger-lab/Tpallidum_WGS. Paired end reads were adapter- and quality-trimmed by Trimmomatic 0.35 (67), using a 4 base sliding window with average quality of 15 and a minimum length of 20, retaining only paired reads. Trimmed reads were then filtered with bbduk v38.86 (68) in two separate steps. First, reads were filtered very stringently,

allowing removal of contaminating non-*T. pallidum* reads, against a reference containing the two rRNA loci, with a 100 bp 5' and 3' flank, from each of five reference *T. pallidum* genomes (NC_021508.1 (*T. pallidum* subsp. *pallidum* strain SS14), NC_016842.1 (*T. pallidum* subsp. *pertenue* strain SamoaD), NC_016843.1 (*T. pallidum* subsp. *pertenue* strain Gauthier), NC_021179 (*T. pallidum* strain Fribourg-Blanc treponeme), NZ_CP034918.1 (*T. pallidum* subsp. *pallidum* strain CW65)). We used a kmer size of 31, a Hamming distance of 1, a minimum of 98% of kmers to match reference, and removal of both reads if either does not pass these criteria. Second, unmatched reads from the rRNA filtration step were then filtered against the complete reference genomes that had been masked with N at the rRNA loci, using a kmer size of 31 and a Hamming distance of 2. Matching reads from the two steps were concatenated and used for input for genome mapping and assembly.

Genome assembly: Filtered reads were mapped to the *T. pallidum* street 14 reference genome, NC_021508.1, using Bowtie2 v2.4.1 (69) with default parameters and coverted to bam with samtools v1.6 (70), followed by deduplication by MarkDuplicates in Picard v2.23.3 (71). Prior to *de novo* assembly, rRNA-stripped reads were filtered with bbduk (68) to remove repetitive regions of the genome, including the repeat regions of the *arp* and *TP0470* genes, as well as *tprC*, *tprD*, and the *tprEGF* and *tprIJ* loci, using a pseudo-kmer size of 45 and Hamming distance of 2. *De novo* assembly was performed using Unicycler v0.4.4 (72) using default settings, with rRNA- and repetitive region-stripped paired fastqs as input. Contigs longer than 200 bp were then mapped back to NC_021508.1 reference genome using bwa-mem 0.7.17-r1188 (73) and a custom R script (74) used to generate a hybrid fasta merging contigs and filling gaps with the reference genome. Deduplicated reads were initially remapped to this hybrid using default Bowtie2 settings, local misalignments corrected with Pilon v1.23.0 (75), and a final

606 Bowtie2 remapping to the Pilon consensus used as input to a custom R script (74) to close gaps
607 and generate a final consensus sequence, with each position called at a threshold of 50% of reads
608 supporting a single base. A minimum of six reads were required to call bases; coverage lower
609 than 6x was left ambiguous by calling "N". All steps of genome generation were visualized and
610 manually confirmed in Geneious Prime v2020.1.2 (76). Following consensus generation, the
611 tRNA-Ile and tRNA-Ala sites that occur within the rRNA loci were masked to N due to short
612 reads being unable to resolve the order of the sites. Consensus genomes were further masked at
613 the *arp* and *tp0470* repeats and *tprK* variable regions prior to further analysis and deposition in
614 the NCBI genome database.
615 **Phylogeny:** Consensus genomes that had been masked at the *arp* and *tp0470* repeats, intra-rRNA
616 tRNAs, and *tprK* variable regions were further masked to N at all *tpr* genes, which are known to
617 be recombinogenic (35). Masked genomes were aligned with MAFFT v7.271 (77) with a gap
618 open penalty of 2.0 and an offset (gap extension penalty) of 0.123. Aligned genomes were
619 recombination masked using 25 iterations of Gubbins v2.4.1 (23). Recombination masking was
620 performed separately with and without *T. pallidum* subsp. *pertenue* and *T. pallidum* subsp.
621 *endemicum* sequences as appropriate. Recombination masking was mapped back onto whole
622 genome sequences and visualized using maskrc-svg v0.5 (78), and iqtree v2.0.3 (79) used to
623 generate a whole genome maximum likelihood phylogeny using 1000 ultrafast bootstraps and
624 automated selection of the best substitution model. A non-recombination-masked maximum
625 likelihood tree was generated using the same parameters but with the raw MAFFT output.
626 Sequences of *tp0136*, *tp0548*, and *tp0705* were extracted and batch queried using the PubMLST
627 database ((32), accessed 01-22-2021).

628 **Bayesian Dating**: TempEst v1.5.3 (80) was used to calculate root-to-tip distances for the SNP-
629 only maximum likelihood phylogeny calculated with or without *T. pallidum* subsp. *pallidum*
630 laboratory strains, assuming one year uncertainty in strains with collection dates estimated.
631 Regressions of distance vs sample date were performed per clade in R. Bayesian dating was
632 performed in the BEAST2 suite (38) using the recombination masked SNP-only (n=600 sites)
633 alignment of *T. pallidum* subsp. *pallidum*, excluding laboratory strains. Priors included a relaxed
634 clock lognormal model with a starting rate of 3.6×10^{-4} (24,39), constant population size, and a
635 GTR +gamma substitution model. Three separate runs, each with 100,000,000 MCMC cycles
636 were performed and the first 10,000,000 cycles discarded as burn-in. All runs converged and
637 were merged prior to calculation of the maximum clade credibility (MCC) tree.
638 **Ancestral node reconstruction**: Augur v10.1.1 (40) was first used to map all tips without
639 recombination masking onto the whole genome phylogeny generated following recombination
640 masking, ensuring appropriate ancestral relationships unconfounded by recombination, using the
641 "refine" function. The "ancestral" function was next used with default settings to infer ancestral
642 node sequences. Sequences of select nodes were aligned to reference NC_021508.1 using
643 MAFFT as above, and annotations of the reference transferred to ancestral node sequences in
644 Geneious. Pairwise global alignments of protein sequences were performed in R using the
645 Biostrings package (81), and analysis and statistical measurements performed in R using custom
646 scripts.
647 **Antigens**: Antigens were manually curated based on being reactive against *T. pallidum* subsp.
648 *pallidum* positive human sera in either of two previous studies (42,43) or, to control for low
649 expression hampering detection by these in vitro methods, by being selected as likely surface
650 proteins or lipoproteins based on extensive literature searches.

651 **Structural modeling**: Genomes were annotated using Prokka v1.14.6 (82), using the --proteins
652 flag to force annotations to comply with NC_021508.1. Translated coding sequences for vaccine-
653 relevant genes were extracted with a custom R script. Sequences containing ambiguities or
654 truncations likely due to assembly gaps in the genome were manually reviewed in Geneious and
655 excluded from further analysis.

656 Homology modelling in RosettaCM (56) was used to build initial models of the SS14
657 variant of each protein. For all sequences collected as part of this study, hhpred (53–55) was
658 used to identify homologous structures, and only those sequences with fulllength alignments
659 (covering >70% of the target) with high probability (>95% hhpred score) were considered for
660 structural modelling. Given these alignments, 100 independent modelling trajectories were
661 carried out for a reference sequence, guided by the top 1-7 templates for each target. We used
662 the following templates in modelling each target: TP0136 used 4a2l and 5oj5; TP0326 used 4k3b
663 and 5d0o; TP0548 used 6h3i; TP0966 used 1yc9, 3d5k, 4k7r, 4mt0, 4mt4, 5azs, and 6u94;
664 TP0967 used 1yc9, 3d5k, 5azp, 5azs, and 6u94. For targets TP0966 and TP0967, modelling was
665 carried out considering the complete homotrimeric configuration, using the symmetry of the
666 templates as a guide.

667 Following homology modelling, the lowest-energy model was selected and used as a
668 starting point for modelling the mutant sequences. We again used RosettaCM, providing the
669 reference model as the “template” and each mutation as the “target” sequence. For each mutant
670 sequence, three models were predicted and the lowest-energy one was used in analysis of
671 structural deviations.

672 Structural deviation analysis involved comparing the structures of proteins with different
673 sequences, and standard difference metrics (like backbone RMSd) do not properly report

differences in sidechain identities. Instead, we used a "per-atom RMSd" metric, where the structures were first superimposed on the reference structure by aligning common backbone atoms. Then, for each atom in the reference structure, the distance was computed not to a corresponding atom, but rather the closest atom of the same chemical identity (e.g., the oxygens of glutamate and aspartate would map to one another). This was then used to calculate the per-atom and per-residue RMS deviations reported in the manuscript. In this part of the analysis, the homotrimeric configuration of targets TP0966 and TP0967 was again used.

Bacterial signal peptide predictions were performed with SignalP 5.0 (58) Linear B cell epitopes were predicted using the BepiPred-2.0 (60).

Statistics and Visualization: Unless otherwise noted, all statistical analysis was performed in R v 4.0.0. Phylogenetic trees and metadata were visualized with the R packages ggtree (83), treeio (84), and ggplot (85), multiple sequence alignments by R package ggmsa (86) and figures generated using cowplot and Adobe Illustrator v24.1.3.

Data Availability: Paired end reads have been uploaded to the NCBI Sequencing Read Archive, Bioproject PRJNA723099. Consensus genomes have been deposited to NCBI Genome, accession numbers CP073381-CP073576 (Supporting Information 1 - Sample Accessions).

Acknowledgements

The authors would like to thank the individuals who donated specimens for the studies conducted here.

References

1. Schmidt R, Carson PJ, Jansen RJ. Resurgence of Syphilis in the United States: An Assessment of Contributing Factors. Infect Dis. 2019;12:1178633719883282.

2. U.S. Department of Health & Human Services. National Overview - Sexually Transmitted Disease Surveillance, 2019 [Internet]. [cited 2021 Apr 19]. Available from: https://www.cdc.gov/std/statistics/2019/overview.htm#Syphilis

3. Kojima N, Klausner JD. An Update on the Global Epidemiology of Syphilis. Curr Epidemiol Rep. 2018 Mar;5(1):24–38.

4. Kanyangarara M, Walker N, Boerma T. Gaps in the implementation of antenatal syphilis detection and treatment in health facilities across sub-Saharan Africa. PloS One. 2018;13(6):e0198622.

5. Korenromp EL, Rowley J, Alonso M, Mello MB, Wijesooriya NS, Mahiané SG, et al. Global burden of maternal and congenital syphilis and associated adverse birth outcomes-Estimates for 2016 and progress since 2012. PloS One. 2019;14(2):e0211720.

6. Nurse-Findlay S, Taylor MM, Savage M, Mello MB, Saliyou S, Lavayen M, et al. Shortages of benzathine penicillin for prevention of mother-to-child transmission of syphilis: An evaluation from multi-country surveys and stakeholder interviews. PLoS Med. 2017 Dec;14(12):e1002473.

7. Stamm LV, Bergen HL. A point mutation associated with bacterial macrolide resistance is present in both 23S rRNA genes of an erythromycin-resistant Treponema pallidum clinical isolate. Antimicrob Agents Chemother. 2000 Mar;44(3):806–7.

716 8. Šmajs D, Paštěková L, Grillová L. Macrolide Resistance in the Syphilis Spirochete,
717 Treponema pallidum ssp. pallidum: Can We Also Expect Macrolide-Resistant Yaws
718 Strains? Am J Trop Med Hyg. 2015 Oct;93(4):678–83.

719 9. Marra CM, Colina AP, Godornes C, Tantalo LC, Puray M, Centurion-Lara A, et al.
720 Antibiotic selection may contribute to increases in macrolide-resistant Treponema pallidum.
721 J Infect Dis. 2006 Dec 15;194(12):1771–3.

722 10. Walker EM, Zampighi GA, Blanco DR, Miller JN, Lovett MA. Demonstration of rare
723 protein in the outer membrane of Treponema pallidum subsp. pallidum by freeze-fracture
724 analysis. J Bacteriol. 1989 Sep;171(9):5005–11.

725 11. Radolf JD. Treponema pallidum and the quest for outer membrane proteins. Mol Microbiol.
726 1995 Jun;16(6):1067–73.

727 12. Giacani L, Brandt SL, Ke W, Reid TB, Molini BJ, Iverson-Cabral S, et al. Transcription of
728 TP0126, Treponema pallidum putative OmpW homolog, is regulated by the length of a
729 homopolymeric guanosine repeat. Infect Immun. 2015 Jun;83(6):2275–89.

730 13. Haynes AM, Fernandez M, Romeis E, Mitjà O, Konda KA, Vargas SK, et al.
731 Transcriptional and immunological analysis of the putative outer membrane protein and
732 vaccine candidate TprL of Treponema pallidum. PLoS Negl Trop Dis. 2021
733 Jan;15(1):e0008812.

734 14. Centurion-Lara A, LaFond RE, Hevner K, Godornes C, Molini BJ, Van Voorhis WC, et al.
735 Gene conversion: a mechanism for generation of heterogeneity in the tprK gene of
736 Treponema pallidum during infection. Mol Microbiol. 2004 Jun;52(6):1579–96.

15. Giacani L, Molini BJ, Kim EY, Godornes BC, Leader BT, Tantalo LC, et al. Antigenic variation in Treponema pallidum: TprK sequence diversity accumulates in response to immune pressure during experimental syphilis. J Immunol Baltim Md 1950. 2010 Apr 1;184(7):3822–9.

16. Reid TB, Molini BJ, Fernandez MC, Lukehart SA. Antigenic variation of TprK facilitates development of secondary syphilis. Infect Immun. 2014 Dec;82(12):4959–67.

17. Edmondson DG, Hu B, Norris SJ. Long-Term In Vitro Culture of the Syphilis Spirochete Treponema pallidum subsp. pallidum. mBio. 2018 Jun 26;9(3).

18. Hopkins S, Lyons F, Coleman C, Courtney G, Bergin C, Mulcahy F. Resurgence in Infectious Syphilis in Ireland: An Epidemiological Study. Sex Transm Dis. 2004 May;31(5):317–21.

19. Lukehart SA, Godornes C, Molini BJ, Sonnett P, Hopkins S, Mulcahy F, et al. Macrolide resistance in Treponema pallidum in the United States and Ireland. N Engl J Med. 2004 Jul 8;351(2):154–8.

20. Marra CM, Sahi SK, Tantalo LC, Godornes C, Reid T, Behets F, et al. Enhanced molecular typing of treponema pallidum: geographical distribution of strain types and association with neurosyphilis. J Infect Dis. 2010 Nov 1;202(9):1380–8.

21. Hook III EW, Behets F, Van Damme K, Ravelomanana N, Leone P, Sena AC, et al. A Phase III Equivalence Trial of Azithromycin versus Benzathine Penicillin for Treatment of Early Syphilis. J Infect Dis. 2010 Jun;201(11):1729–35.

757 22. Van Damme K, Behets F, Ravelomanana N, Godornes C, Khan M, Randrianasolo B, et al.
758 Evaluation of Azithromycin Resistance in Treponema pallidum Specimens From
759 Madagascar. Sex Transm Dis. 2009 Dec;36(12):775–6.

760 23. Croucher NJ, Page AJ, Connor TR, Delaney AJ, Keane JA, Bentley SD, et al. Rapid
761 phylogenetic analysis of large samples of recombinant bacterial whole genome sequences
762 using Gubbins. Nucleic Acids Res. 2015 Feb 18;43(3):e15.

763 24. Beale MA, Marks M, Sahi SK, Tantalo LC, Nori AV, French P, et al. Genomic
764 epidemiology of syphilis reveals independent emergence of macrolide resistance across
765 multiple circulating lineages. Nat Commun. 2019 Jul 22;10(1):3255.

766 25. Grimes M, Sahi SK, Godornes BC, Tantalo LC, Roberts N, Bostick D, et al. Two mutations
767 associated with macrolide resistance in Treponema pallidum: increasing prevalence and
768 correlation with molecular strain type in Seattle, Washington. Sex Transm Dis. 2012
769 Dec;39(12):954–8.

770 26. Nishiki S, Lee K, Kanai M, Nakayama S-I, Ohnishi M. Phylogenetic and genetic
771 characterization of Treponema pallidum strains from syphilis patients in Japan by whole-
772 genome sequence analysis from global perspectives. Sci Rep. 2021 Feb 4;11(1):3154.

773 27. Pětrošová H, Zobaníková M, Čejková D, Mikalová L, Pospíšilová P, Strouhal M, et al.
774 Whole genome sequence of Treponema pallidum ssp. pallidum, strain Mexico A, suggests
775 recombination between yaws and syphilis strains. PLoS Negl Trop Dis. 2012;6(9):e1832.

776 28. Centurion-Lara A, Giacani L, Godornes C, Molini BJ, Brinck Reid T, Lukehart SA. Fine
777 analysis of genetic diversity of the tpr gene family among treponemal species, subspecies
778 and strains. PLoS Negl Trop Dis. 2013;7(5):e2222.

779 29. Kawahata T, Kojima Y, Furubayashi K, Shinohara K, Shimizu T, Komano J, et al. Bejel, a
780 Nonvenereal Treponematosis, among Men Who Have Sex with Men, Japan. Emerg Infect
781 Dis. 2019 Aug;25(8):1581–3.

782 30. Noda AA, Grillová L, Lienhard R, Blanco O, Rodríguez I, Šmajs D. Bejel in Cuba:
783 molecular identification of Treponema pallidum subsp. endemicum in patients diagnosed
784 with venereal syphilis. Clin Microbiol Infect Off Publ Eur Soc Clin Microbiol Infect Dis.
785 2018 Nov;24(11):1210.e1-1210.e5.

786 31. Mikalová L, Strouhal M, Oppelt J, Grange PA, Janier M, Benhaddou N, et al. Human
787 Treponema pallidum 11q/j isolate belongs to subsp. endemicum but contains two loci with
788 a sequence in TP0548 and TP0488 similar to subsp. pertenue and subsp. pallidum,
789 respectively. PLoS Negl Trop Dis. 2017 Mar;11(3):e0005434.

790 32. Grillova L, Jolley K, Šmajs D, Picardeau M. A public database for the new MLST scheme
791 for Treponema pallidum subsp. pallidum: surveillance and epidemiology of the causative
792 agent of syphilis. PeerJ. 2019;6:e6182.

793 33. Grillová L, Oppelt J, Mikalová L, Nováková M, Giacani L, Niesnerová A, et al. Directly
794 Sequenced Genomes of Contemporary Strains of Syphilis Reveal Recombination-Driven
795 Diversity in Genes Encoding Predicted Surface-Exposed Antigens. Front Microbiol.
796 2019;10:1691.

34. Kumar S, Caimano MJ, Anand A, Dey A, Hawley KL, LeDoyt ME, et al. Sequence Variation of Rare Outer Membrane Protein β-Barrel Domains in Clinical Strains Provides Insights into the Evolution of Treponema pallidum subsp. pallidum, the Syphilis Spirochete. mBio. 2018 Jun 12;9(3).

35. Gray RR, Mulligan CJ, Molini BJ, Sun ES, Giacani L, Godornes C, et al. Molecular evolution of the tprC, D, I, K, G, and J genes in the pathogenic genus Treponema. Mol Biol Evol. 2006 Nov;23(11):2220–33.

36. Majander K, Pfrengle S, Kocher A, Neukamm J, du Plessis L, Pla-Díaz M, et al. Ancient Bacterial Genomes Reveal a High Diversity of Treponema pallidum Strains in Early Modern Europe. Curr Biol CB. 2020 Oct 5;30(19):3788-3803.e10.

37. Zobaníková M, Strouhal M, Mikalová L, Cejková D, Ambrožová L, Pospíšilová P, et al. Whole genome sequence of the Treponema Fribourg-Blanc: unspecified simian isolate is highly similar to the yaws subspecies. PLoS Negl Trop Dis. 2013;7(4):e2172.

38. Bouckaert R, Vaughan TG, Barido-Sottani J, Duchêne S, Fourment M, Gavryushkina A, et al. BEAST 2.5: An advanced software platform for Bayesian evolutionary analysis. PLoS Comput Biol. 2019 Apr;15(4):e1006650.

39. Arora N, Schuenemann VJ, Jäger G, Peltzer A, Seitz A, Herbig A, et al. Origin of modern syphilis and emergence of a pandemic Treponema pallidum cluster. Nat Microbiol. 2017 Jan;2(1):16245.

816 40. Huddleston J, Hadfield J, Sibley T, Lee J, Fay K, Ilcisin M, et al. Augur: a bioinformatics
817 toolkit for phylogenetic analyses of human pathogens. J Open Source Softw. 2021 Jan
818 7;6(57):2906.

819 41. Houston S, Lithgow KV, Osbak KK, Kenyon CR, Cameron CE. Functional insights from
820 proteome-wide structural modeling of Treponema pallidum subspecies pallidum, the
821 causative agent of syphilis. BMC Struct Biol. 2018 May 16;18(1):7.

822 42. Brinkman MB, McKevitt M, McLoughlin M, Perez C, Howell J, Weinstock GM, et al.
823 Reactivity of antibodies from syphilis patients to a protein array representing the
824 Treponema pallidum proteome. J Clin Microbiol. 2006 Mar;44(3):888–91.

825 43. McGill MA, Edmondson DG, Carroll JA, Cook RG, Orkiszewski RS, Norris SJ.
826 Characterization and serologic analysis of the Treponema pallidum proteome. Infect
827 Immun. 2010 Jun;78(6):2631–43.

828 44. Subramanian G, Koonin EV, Aravind L. Comparative genome analysis of the pathogenic
829 spirochetes Borrelia burgdorferi and Treponema pallidum. Infect Immun. 2000
830 Mar;68(3):1633–48.

831 45. Hawley KL, Montezuma-Rusca JM, Delgado KN, Singh N, Uversky VN, Caimano MJ, et
832 al. Structural modeling of the Treponema pallidum OMPeome: a roadmap for
833 deconvolution of syphilis pathogenesis and development of a syphilis vaccine. J Bacteriol.
834 2021 May 10;

835 46. Radolf JD, Kumar S. The Treponema pallidum Outer Membrane. Curr Top Microbiol
836 Immunol. 2018;415:1–38.

837 47. Brinkman MB, McGill MA, Pettersson J, Rogers A, Matejková P, Smajs D, et al. A novel
838 Treponema pallidum antigen, TP0136, is an outer membrane protein that binds human
839 fibronectin. Infect Immun. 2008 May;76(5):1848–57.

840 48. Djokic V, Giacani L, Parveen N. Analysis of host cell binding specificity mediated by the
841 Tp0136 adhesin of the syphilis agent Treponema pallidum subsp. pallidum. PLoS Negl
842 Trop Dis. 2019 May;13(5):e0007401.

843 49. Ke W, Molini BJ, Lukehart SA, Giacani L. Treponema pallidum subsp. pallidum TP0136
844 Protein Is Heterogeneous among Isolates and Binds Cellular and Plasma Fibronectin via its
845 NH2-Terminal End. Picardeau M, editor. PLoS Negl Trop Dis. 2015 Mar
846 20;9(3):e0003662.

847 50. Cameron CE, Lukehart SA, Castro C, Molini B, Godornes C, Van Voorhis WC. Opsonic
848 potential, protective capacity, and sequence conservation of the Treponema pallidum
849 subspecies pallidum Tp92. J Infect Dis. 2000 Apr;181(4):1401–13.

850 51. Zhao F, Wu Y, Zhang X, Yu J, Gu W, Liu S, et al. Enhanced immune response and
851 protective efficacy of a Treponema pallidum Tp92 DNA vaccine vectored by chitosan
852 nanoparticles and adjuvanted with IL-2. Hum Vaccin. 2011 Oct;7(10):1083–9.

853 52. Tomson FL, Conley PG, Norgard MV, Hagman KE. Assessment of cell-surface exposure
854 and vaccinogenic potentials of Treponema pallidum candidate outer membrane proteins.
855 Microbes Infect. 2007 Sep;9(11):1267–75.

856 53. Zimmermann L, Stephens A, Nam S-Z, Rau D, Kübler J, Lozajic M, et al. A Completely
857 Reimplemented MPI Bioinformatics Toolkit with a New HHpred Server at its Core. J Mol
858 Biol. 2018 Jul;430(15):2237–43.

859 54. Gabler F, Nam S, Till S, Mirdita M, Steinegger M, Söding J, et al. Protein Sequence
860 Analysis Using the MPI Bioinformatics Toolkit. Curr Protoc Bioinforma [Internet]. 2020
861 Dec [cited 2021 Jun 7];72(1). Available from:
862 https://onlinelibrary.wiley.com/doi/10.1002/cpbi.108

863 55. Söding J, Biegert A, Lupas AN. The HHpred interactive server for protein homology
864 detection and structure prediction. Nucleic Acids Res. 2005 Jul 1;33(Web Server
865 issue):W244-248.

866 56. Song Y, DiMaio F, Wang RY-R, Kim D, Miles C, Brunette T, et al. High-Resolution
867 Comparative Modeling with RosettaCM. Structure. 2013 Oct;21(10):1735–42.

868 57. Desrosiers DC, Anand A, Luthra A, Dunham-Ems SM, LeDoyt M, Cummings MAD, et al.
869 TP0326, a Treponema pallidum β-barrel assembly machinery A (BamA) orthologue and
870 rare outer membrane protein. Mol Microbiol. 2011 Jun;80(6):1496–515.

871 58. Almagro Armenteros JJ, Tsirigos KD, Sønderby CK, Petersen TN, Winther O, Brunak S, et
872 al. SignalP 5.0 improves signal peptide predictions using deep neural networks. Nat
873 Biotechnol. 2019 Apr;37(4):420–3.

874 59. Luthra A, Anand A, Hawley KL, LeDoyt M, La Vake CJ, Caimano MJ, et al. A Homology
875 Model Reveals Novel Structural Features and an Immunodominant Surface Loop/Opsonic

Target in the Treponema pallidum BamA Ortholog TP_0326. J Bacteriol. 2015 Jun;197(11):1906–20.

60. Jespersen MC, Peters B, Nielsen M, Marcatili P. BepiPred-2.0: improving sequence-based B-cell epitope prediction using conformational epitopes. Nucleic Acids Res. 2017 Jul 3;45(W1):W24–9.

61. Chouhan B, Denesyuk A, Heino J, Johnson MS, Denessiouk K. Conservation of the human integrin-type beta-propeller domain in bacteria. PloS One. 2011;6(10):e25069.

62. Bonnardel F, Kumar A, Wimmerova M, Lahmann M, Perez S, Varrot A, et al. Architecture and Evolution of Blade Assembly in β-propeller Lectins. Structure. 2019 May;27(5):764-775.e3.

63. Beale MA, Marks M, Cole MJ, Lee M-K, Pitt R, Ruis C, et al. Contemporary syphilis is characterised by rapid global spread of pandemic *Treponema pallidum* lineages [Internet]. Infectious Diseases (except HIV/AIDS); 2021 Mar [cited 2021 Jun 8]. Available from: http://medrxiv.org/lookup/doi/10.1101/2021.03.25.21250180

64. Titz B, Rajagopala SV, Goll J, Häuser R, McKevitt MT, Palzkill T, et al. The binary protein interactome of Treponema pallidum--the syphilis spirochete. PloS One. 2008 May 28;3(5):e2292.

65. Romeis E, Tantalo L, Lieberman N, Phung Q, Greninger A, Giacani L. Genetic Engineering of *Treponema pallidum* subsp. *pallidum* , the Syphilis Spirochete [Internet]. Microbiology; 2021 May [cited 2021 Jun 10]. Available from: http://biorxiv.org/lookup/doi/10.1101/2021.05.07.443079

66. Addetia A, Lin MJ, Phung Q, Xie H, Huang M-L, Ciccarese G, et al. Estimation of Full-Length TprK Diversity in Treponema pallidum subsp. *pallidum*. Norris SJ, editor. mBio [Internet]. 2020 Oct 27 [cited 2021 Jun 7];11(5). Available from: https://journals.asm.org/doi/10.1128/mBio.02726-20

67. Bolger AM, Lohse M, Usadel B. Trimmomatic: a flexible trimmer for Illumina sequence data. Bioinforma Oxf Engl. 2014 Aug 1;30(15):2114–20.

68. Bushnell B. BBMap short read aligner, and other bioinformatic tools.

69. Langmead B, Salzberg SL. Fast gapped-read alignment with Bowtie 2. Nat Methods. 2012 Apr;9(4):357–9.

70. Li H, Handsaker B, Wysoker A, Fennell T, Ruan J, Homer N, et al. The Sequence Alignment/Map format and SAMtools. Bioinformatics. 2009 Aug 15;25(16):2078–9.

71. Broad Institute. Picard [Internet]. Available from: http://broadinstitute.github.io/picard.

72. Wick RR, Judd LM, Gorrie CL, Holt KE. Unicycler: Resolving bacterial genome assemblies from short and long sequencing reads. Phillippy AM, editor. PLOS Comput Biol. 2017 Jun 8;13(6):e1005595.

73. Li H, Durbin R. Fast and accurate short read alignment with Burrows-Wheeler transform. Bioinforma Oxf Engl. 2009 Jul 15;25(14):1754–60.

74. Greninger AL, Roychoudhury P, Xie H, Casto A, Cent A, Pepper G, et al. Ultrasensitive Capture of Human Herpes Simplex Virus Genomes Directly from Clinical Samples Reveals Extraordinarily Limited Evolution in Cell Culture. mSphere. 2018 Jun 27;3(3).

75. Walker BJ, Abeel T, Shea T, Priest M, Abouelliel A, Sakthikumar S, et al. Pilon: An Integrated Tool for Comprehensive Microbial Variant Detection and Genome Assembly Improvement. Wang J, editor. PLoS ONE. 2014 Nov 19;9(11):e112963.

76. Geneious. Geneious [Internet]. Available from: https://www.geneious.com

77. Katoh K, Standley DM. MAFFT Multiple Sequence Alignment Software Version 7: Improvements in Performance and Usability. Mol Biol Evol. 2013 Apr 1;30(4):772–80.

78. Kwong J, Seemann T. maskrc-svg [Internet]. Available from: https://github.com/kwongj/maskrc-svg

79. Nguyen L-T, Schmidt HA, von Haeseler A, Minh BQ. IQ-TREE: A Fast and Effective Stochastic Algorithm for Estimating Maximum-Likelihood Phylogenies. Mol Biol Evol. 2015 Jan;32(1):268–74.

80. Rambaut A, Lam TT, Max Carvalho L, Pybus OG. Exploring the temporal structure of heterochronous sequences using TempEst (formerly Path-O-Gen). Virus Evol. 2016 Jan;2(1):vew007.

81. Pages H, Aboyoun P, Gentleman R, DebRoy S. Biostrings: Efficient manipulation of biological strings. R package version 2.60.1 [Internet]. Available from: https://bioconductor.org/packages/Biostrings

82. Seemann T. Prokka: rapid prokaryotic genome annotation. Bioinforma Oxf Engl. 2014 Jul 15;30(14):2068–9.

936 83. Yu G, Smith DK, Zhu H, Guan Y, Lam TT. ggtree: an R package for visualization and
937 annotation of phylogenetic trees with their covariates and other associated data. McInerny
938 G, editor. Methods Ecol Evol. 2017 Jan;8(1):28–36.

939 84. Wang L-G, Lam TT-Y, Xu S, Dai Z, Zhou L, Feng T, et al. Treeio: An R Package for
940 Phylogenetic Tree Input and Output with Richly Annotated and Associated Data. Kumar S,
941 editor. Mol Biol Evol. 2020 Feb 1;37(2):599–603.

942 85. Wickham H. ggplot2: Elegant Graphics for Data Analysis. 2nd ed. 2016. Cham: Springer
943 International Publishing : Imprint: Springer; 2016. 1 p. (Use R!).

944 86. Yu G, Zhou L, Xu S, Huang H. ggmsa 1.0.0. [cited 2021 Jul 11]. Available from:
945 http://yulab-smu.top/ggmsa/authors.html

946

947 **Figure Legends:**

948 **Figure 1: Whole genome phylogeny of *T. pallidum* patient isolates.** A) Whole genomes were
949 MAFFT-aligned, recombination-masked, and maximum-likelihood phylogeny determined. Tips
950 are shown as grey triangles and nodes with >0.95 support from 1000 ultrafast bootstraps shown
951 as black circles. B) Subspecies/lineage, subclade, and continent of origin of all samples included
952 in phylogeny. C) Azithromycin sensitivity/resistance as conferred by the 23S rRNA 2058/2059
953 alleles. Data represents alleles at both rRNA loci. D) MLST subtypes, including novel
954 sequences, for *tp0136*, *tp0548*, and *tp0705*, as well as whether the three alleles constitute a
955 known or novel MLST. Top 6 most abundant sequences at each locus are colored, while other
956 less abundant known and novel sequences are grouped and colored in light and medium grey,

957 respectively. Sequences containing N bases are denoted as indeterminate and shown in dark
958 grey. Expanded metadata for all samples is included in Supporting Information 1.
959
960 **Figure 2: Effect of recombination on *T. pallidum* subsp. *pallidum* evolution**. A)
961 Recombination-masked (left) and unmasked (right) phylogenies, with equivalent subclades
962 highlighted. Relative position of each tip is traced between the two panels. B) Putative
963 recombinogenic regions in each clade. Genomic position is relative to the length of the MAFFT
964 alignment. Consensus alignment of all tips is shown on the grey panel, with recombination
965 blocks lettered above. Grey blocks represent recombination that occurred during evolution of the
966 SS14 clade. Red and blue blocks represent recombination events unique to each clade. Mixed
967 grey and colored blocks are regions of ancestral recombination that had a second event unique to
968 that clade. C-F) Two example regions of recombination in SS14 Mexico (C), Nichols A (D),
969 Nichols B (E), and Nichols E (F). Genomic position of the first divergent base in the window
970 shown are shown with NC_021508.1 numbering.
971
972 **Figure 3: SS14 and Nichols subclades have different rates of SNP accumulation.** A) Linear
973 regressions for recombination-masked root-to-tip distances from maximum likelihood phylogeny
974 as a function of year of collection, including (left) or not including (right) highly passaged
975 laboratory strains. B) Residuals from linear regression without laboratory strains were plotted per
976 subclade, $p < 2e^{-16}$, ANOVA. C) Bayesian maximum clade credibility tree showing mean
977 common ancestor heights. Highlighted nodes have a posterior probability of >0.95, and branch
978 colors reveal rate of change (SNPs per genome per year). Ages and 95% highest posterior
979 density are included for nodes of interest including the TPA, SS14, and Nichols ancestral nodes,

as well as those of each subclade. Inset: For each tip, mean rates of SNP accumulation along branches with >0.95 posterior probability were plotted per subclade, $p < 2e^{-16}$, ANOVA.

Figure 4: Coding mutations in the *T. pallidum* subsp. *pallidum* phylogeny. A) Whole genome ML phylogeny of TPA, with tips collapsed to the subclade node. Open reading frames of inferred ancestral sequences for each node were annotated based on the SS14 reference sequence NC_021508. Coding mutations, including for putative recombinant genes, for each child node were determined relative to its parent node (complete list in Supporting Information 4). Loci with amino acid differences (n=49 loci, n=134 individual AA mutation events) in the SS14 ancestral clade node (N101) are shown relative to the Nichols ancestral node (N001). B) Positions are equivalent to those shown in A. Black square represents the Nichols Ancestral Node (N001). Number of antigens with coding mutations on each child node relative to parent node. Color represents p value of for overrepresentation by Fisher's Exact test of antigens among all mutated proteins per branch; those in grey have a p value > 0.05. C) Percentage of total individual mutation events per branch. Raw numbers of mutation events in antigens per total mutation events are shown for each branch. D) Tile plot showing mutated proteins in the ancestral node for each subclade relative to its parent node, colored by antigen or not. Proteins are arranged by number of subclades bearing mutations. Data is recapitulated in Supporting Information 3

Supplementary Figure 1: Distribution of putative protein functional annotation based on high-confidence Phyre2 models. Percent of proteins in each category different between the SS14 ancestral clade node (N101) and the Nichols ancestral node (N001) (orange) were

compared to annotations across the whole genome (purple). Overrepresentation was tested by Fisher's exact test, $*p < 0.05$.

Supplementary Figure 2: Multiple sequence alignment and structural modeling of TP0326. A) Multiple sequence alignment for all amino acid sequence variants. Polymorphic residues are highlighted, and positions of extracellular loops 3, 4, and 7 are shown. B) Side (left) and top (right) cartoon representation of TP0326, with a color gradient between blue at the N-terminus to red at the C-terminus. C) Side (left) and top (right) space-filling representation of TP0326, with polymorphic residue positions colored magenta. D) Side (left) and top (right) space-filling representation of TP0326, with atoms colored by average per atom displacement in all variants relative to the SS14 reference sequence. Arrows, single arrowheads, and double arrowheads point to positions of ECLs 4, 7, and 3, respectively.

Supplementary Figure 3: Multiple sequence alignment and structural modeling of TP0548. A) Multiple sequence alignment for all amino acid sequence variants. Polymorphic residues are highlighted, and positions of relevant predicted B cell epitopes are shown. B) Side (left) and top (right) cartoon representation of TP0548, with a color gradient between blue at the N-terminus to red at the C-terminus. Arrows point to the flexible loops that contain predicted linear BCEs. C) Side (left) and top (right) space-filling representation of TP0548, with polymorphic residue positions colored magenta. D) Side (left) and top (right) space-filling representation of TP0966, with atoms colored by average per atom displacement in all variants relative to the SS14 reference sequence. Arrow points to ECL-2, which contains two invariant predicted BCEs.

Supplementary Figure 4: Multiple sequence alignment and structural modeling of TP0966. A) Multiple sequence alignment for all amino acid sequence variants. Polymorphic residues are highlighted. ECLs 1 and 2 are boxed, and the linear BCEs contained in the SS14 variant (#1) are marked in red. B) Side (left) and top (right) cartoon representation of TP0966, with a color gradient between blue at the N-terminus to red at the C-terminus. C) Side (left) and top (right) space-filling representation of TP0966, with polymorphic residue positions colored magenta. Arrow points to polymorphic residues in surface loops. D) Side (left) and top (right) space-filling representation of TP0966, with atoms colored by average per atom displacement in all variants relative to the SS14 reference sequence. Arrows point to the high displacement, non-polymorphic residues.

Supplementary Figure 5: Multiple sequence alignment and structural modeling of TP0967. A) Multiple sequence alignment for all amino acid sequence variants. Polymorphic residues are highlighted. ECL1 is boxed, and the linear BCE contained in the SS14 variant (#4) is marked in red. B) Side (left) and top (right) cartoon representation of TP0967, with a color gradient between blue at the N-terminus to red at the C-terminus. C) Side (left) and top (right) space-filling representation of TP0967, with polymorphic residue positions colored magenta. Arrow points to polymorphic residues in surface loops. D) Side (left) and top (right) space-filling representation of TP0967, with atoms colored by average per atom displacement in all variants relative to the SS14 reference sequence. Arrows point to the high displacement, non-polymorphic residues.

Supplementary Figure 6: Multiple sequence alignment and structural modeling of TP0136. A) Multiple sequence alignment for all amino acid sequence variants. Polymorphic residues are highlighted. B) Side (left) and top (right) cartoon representation of TP0136, with a color gradient between blue at the N-terminus to red at the C-terminus. C) Side (left) and top (right) space-filling representation of TP0136, with polymorphic residue positions colored magenta. D) Side (left) and top (right) space-filling representation of TP0136, with atoms colored by average per atom displacement in all variants relative to the SS14 reference sequence. Boxed areas represent regions of low displacement in the β-strands. In all panels, arrows point to the large extracellular loop that is removed in variants found in several subclades.

Supporting Information 1: Expanded metadata for all samples presented in Figure 1.

Sample Statistics: "Input Genomes" refers to the number of copies of TP47 (*tp0574*) included in pre-capture library preparation. "Coverage" refers to the average deduplicated read depth at any position in the initial mapping of reads to the reference sequence NC_021508. "Length" is the length of the final consensus genome. "Number Ambiguities" and "Percent Ambiguities" refers to Ns in samples prior to masking. ***Sample Accessions***: NCBI Biosample and assembly accessions per sample. ***Sample Metadata:*** "Tip Number" refers to sample position on the phylogenetic tree in Figure 1, with #1 at the bottom of the page. ***tp0136 MLST, tp0548 MLST, tp0705 MLST:*** *Complete* information on MLST alleles, including how novel sequences relate to the closest known match.

Supporting Information 2: Expanded Recombination Data from Figure 2: *Tip Order:* Top to bottom order of tips in recombination masked and unmasked phylogenies. ***Recombination***

Blocks: Genes included in each recombination block. ***Blocks per Clade***: Precise locations of recombination events detected per clade.

Supporting Information 3: Expanded data for Figure 4. ***Summary Data by Locus:*** Information on number of mutations per locus per branch, including functional annotations. ***Antigens:*** List of loci included as antigens. CDS name and genomic position information is from NC_021508.1. ***Heatmap Data:*** Data included in Figure 4D. "Sum" represents the number of nodes at which there is a change in that locus. ***NXXX vs NYYY:*** Detailed information on all detected mutations per branch, named by parent and child node number.

Supporting Information 4: Expanded data for Supplementary Figures 2-6. TP0136, TP0326, TP0548, TP0966, and TP0967 variant amino acid sequence by sample and subclade.

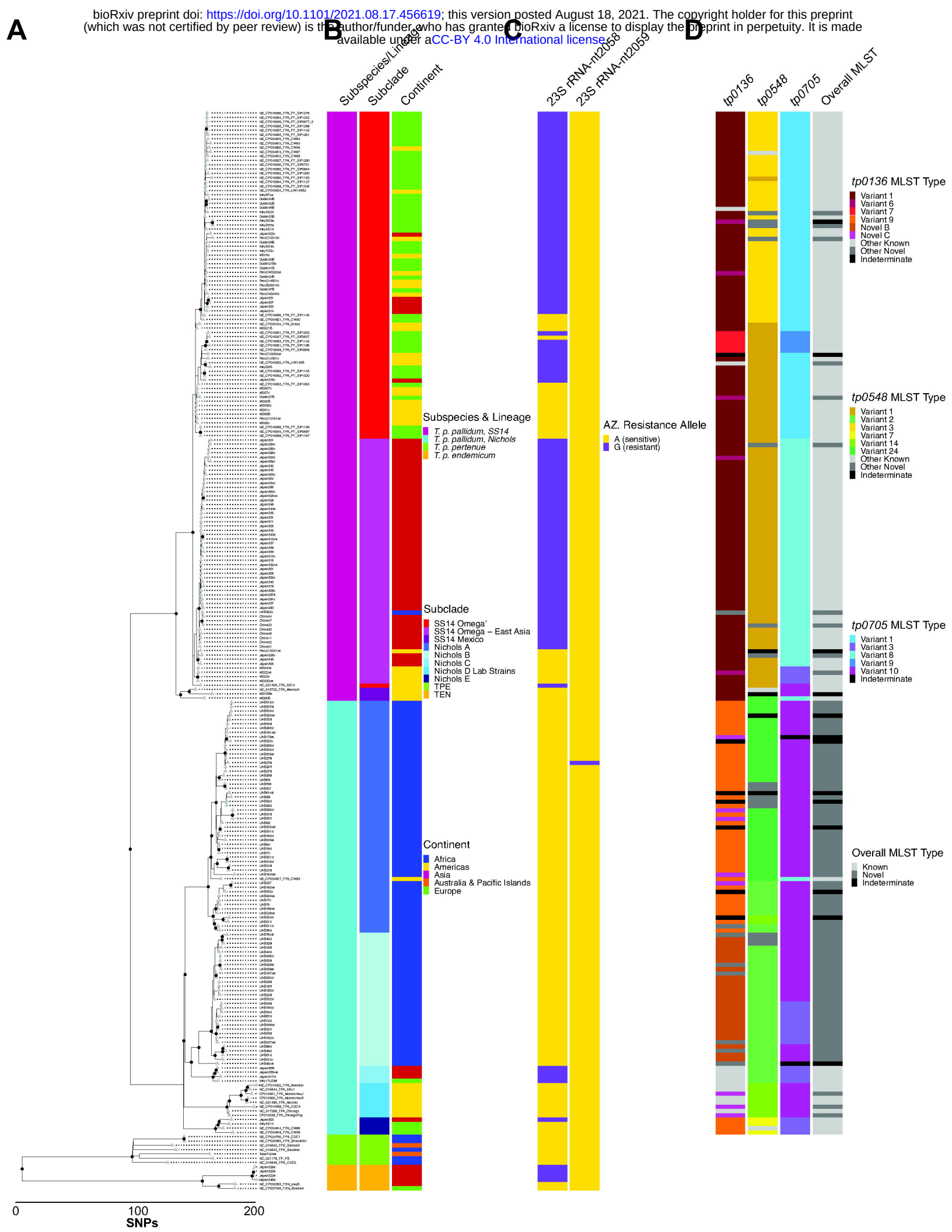

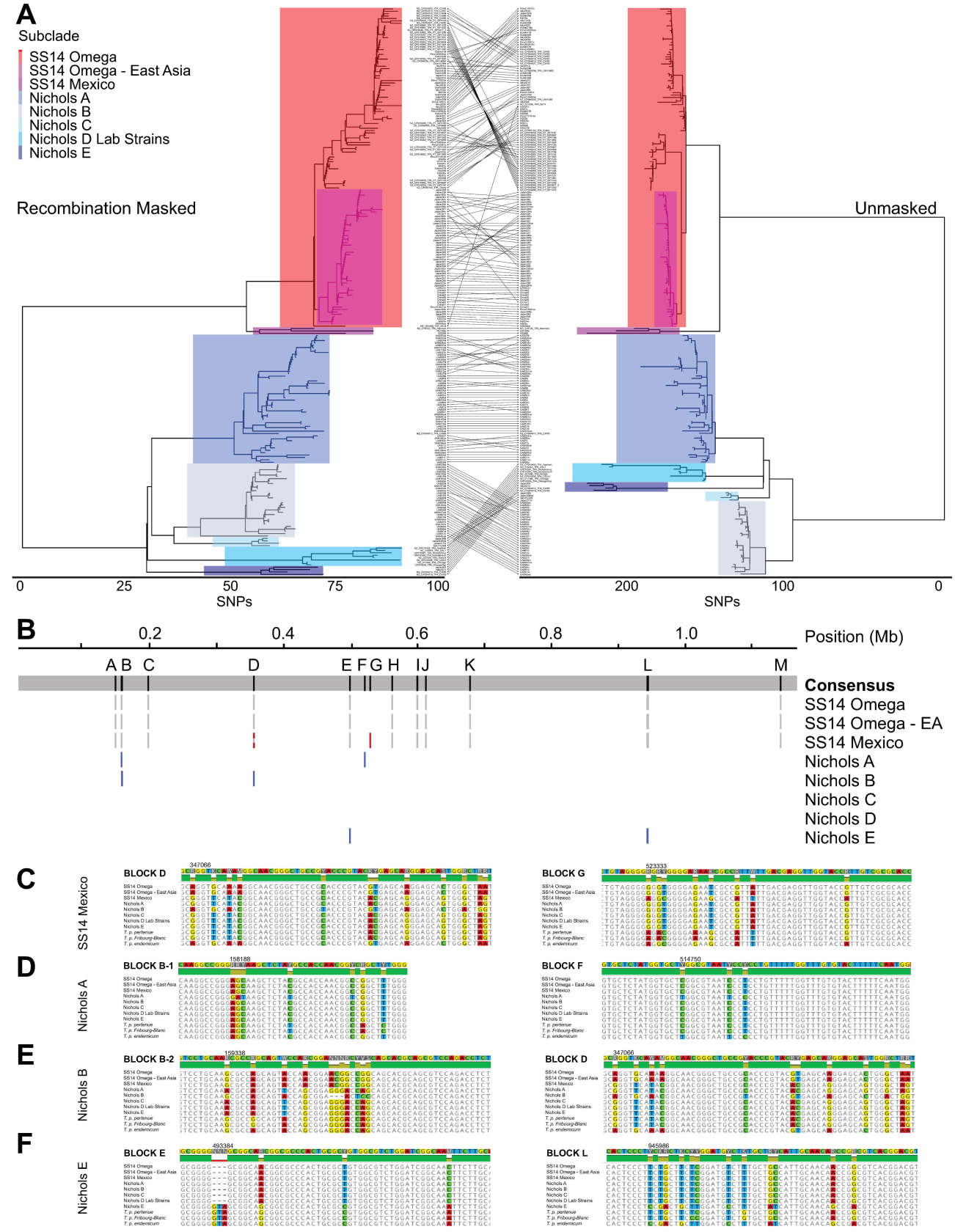
A
Subclade
SS14 Omega
SS14 Omega - East Asia
SS14 Mexico
Nichols A
Nichols B
Nichols C
Nichols D Lab Strains
Nichols E
Recombination Masked
Unmasked
0
25
50
75
100
SNPs
200
100
0
SNPs
B
0.2
0.4
0.6
0.8
1.0
Position (Mb)
A B C
D
E F G H
IJ
K
L
M
Consensus
SS14 Omega
SS14 Omega - EA
SS14 Mexico
Nichols A
Nichols B
Nichols C
Nichols D
Nichols E
C
SS14 Mexico
BLOCK D
347066
BLOCK G
523333
D
Nichols A
BLOCK B-1
158188
BLOCK F
514750
E
Nichols B
BLOCK B-2
159338
BLOCK D
347066
F
Nichols E
BLOCK E
493384
BLOCK L
945986